

Three-Point Correlation Functions of SDSS Galaxies in Redshift Space: Morphology, Color, and Luminosity Dependence

Issha KAYO,^{1*} Yasushi SUTO,¹ Robert C. NICHOL,² Jun PAN,³ István SZAPUDI,³
Andrew J. CONNOLLY,⁴ Jeff GARDNER,^{4,5} Bhuvnesh JAIN,⁶ Gauri KULKARNI,²
Takahiko MATSUBARA,⁷ Ravi SHETH,⁴ Alexander S. SZALAY,⁸ and Jon BRINKMANN⁹

¹*Department of Physics, School of Science, The University of Tokyo, Tokyo 113-0033*

²*Department of Physics, Carnegie Mellon University, 5000 Forbes Avenue, Pittsburgh, PA 15213, USA*

³*Institute for Astronomy, University of Hawaii, 2680 Woodlawn Drive, Honolulu, HI 96822, USA*

⁴*Department of Physics and Astronomy, University of Pittsburgh, 3941 O'Hara Street, Pittsburgh, PA 15260, USA*

⁵*Pittsburgh Supercomputing Center, 4400 Fifth Ave., Pittsburgh, PA 15213, USA*

⁶*Department of Physics, University of Pennsylvania, Philadelphia, PA 19101, USA*

⁷*Department of Physics and Astrophysics, Nagoya University, Chikusa, Nagoya 161-8602*

⁸*Department of Physics and Astronomy, The Johns Hopkins University,
3701 San Martin Drive, Baltimore, MD 21218, USA*

⁹*Apache Point Observatory, Sunspot, NM 88349-0059, USA*

*kayo@phys.nagoya-u.ac.jp, suto@phys.s.u-tokyo.ac.jp, nichol@cmu.edu, jpan@ifa.hawaii.edu,
szapudi@ifa.hawaii.edu, ajc@phyast.pitt.edu, gardner@phyast.pitt.edu, bjain@hep.upenn.edu,*

gkulkarni@andrew.cmu.edu, taka@phys.nagoya-u.ac.jp, sheth@sheth.phyast.pitt.edu, szalay@jhu.edu, jb@apo.nmsu.edu

(Received 2004 March 14; accepted 2004 April 13)

Abstract

We present measurements of the redshift–space three-point correlation function of galaxies in the Sloan Digital Sky Survey (SDSS). For the first time, we analyze the dependence of this statistic on galaxy morphology, color, and luminosity. In order to control systematics due to selection effects, we used r -band, volume-limited samples of galaxies, constructed from magnitude-limited SDSS data ($14.5 < r < 17.5$), and further divided the samples into two morphological types (early and late) or two color populations (red and blue). The three-point correlation function of SDSS galaxies follows the hierarchical relation well, and the reduced three-point amplitudes in redshift–space are almost scale-independent ($Q_z = 0.5 \sim 1.0$). In addition, their dependence on the morphology, color, and luminosity is not statistically significant. Given the robust morphological, color and luminosity dependences of the two-point correlation function, this implies that galaxy biasing is complex on weakly non-linear to non-linear scales. We show that a simple deterministic linear relation with the underlying mass could not explain our measurements on these scales.

Key words: cosmology: large-scale structure of universe — cosmology: observations — methods: statistical

1. Introduction

While the first-year WMAP (Wilkinson Microwave Anisotropy Probe) data imply that the primordial density fluctuations at $z \approx 1000$ are virtually Gaussian (Komatsu et al. 2003), the present structure traced by galaxies shows significant non-Gaussianity. Such non-Gaussian features naturally arise during the course of nonlinear gravitational evolution of dark-matter density fields, the formation of luminous galaxies and their subsequent evolution. Therefore, the degree and nature of non-Gaussian signatures in the galaxy distribution will provide important empirical constraints on the physics of galaxy formation. The three-point correlation function (3PCF) is the lowest-order unambiguous statistic to characterize such non-Gaussianities.

The determination of the 3PCF of galaxies was pioneered by Peebles and Groth (1975) using the Lick and Zwicky angular catalogs of galaxies. Groth and Peebles (1977) found that the 3PCF $\zeta(r_{12}, r_{23}, r_{31})$ obeys the following *hierarchical relation*:

$$\zeta(r_{12}, r_{23}, r_{31}) = Q_r [\xi(r_{12})\xi(r_{23}) + \xi(r_{23})\xi(r_{31}) + \xi(r_{31})\xi(r_{12})], \quad (1)$$

with Q_r being a constant, and $\xi(r)$ is the two-point correlation function (2PCF). The value of Q_r in real space de-projected from these angular catalogues is 1.29 ± 0.21 for $r \lesssim 3h^{-1}$ Mpc. Although subsequent analyses of redshift catalogs confirmed the hierarchical relation, at least approximately, the value of Q_z (in redshift space) appears to be smaller, $0.5 \sim 1$ (Bean et al. 1983; Hale-Sutton et al. 1989; Jing, Börner 1998). Recently, Jing and Börner (2003) have studied the luminosity dependence of Q , and found a small, but significant, trend that brighter galaxies tend to have a lower amplitude than fainter ones.

* Present address: Department of Physics and Astrophysics, Nagoya University, Nagoya 464-8602

N-body simulations and perturbative analysis generally predict that the 3PCF should depart from the hierarchical relation, especially on non-linear scales (Fry 1984; Suto, Matsubara 1994; Jing, Börner 1997; Barriga, Gaztañaga 2002). However, Matsubara & Suto (1994) demonstrated that redshift distortions substantially reduce the scale-dependence of Q_r , resulting in Q_z (Q in redshift space) being nearly constant. Still, the amplitude of the Q_z of galaxies is roughly (50% ~ 100%) smaller than predicted by N-body simulations. The discrepancy is likely to be the effect of biasing. Recently, Takada and Jain (2003) proposed a phenomenological model to predict the 3PCF as a function of the galaxy properties, which is based on the halo model. They argue that the color dependence of Q_r should be strong, i.e., the galaxy biasing severely affects the 3PCFs.

There are several statistics that are closely related to the 3PCF, e.g., the reduced moments of counts in cells, such as skewness and kurtosis (see Szapudi et al. 2002, 2004 in preparation). Another similar statistics is the bispectrum, which is the Fourier counterpart of the 3PCF. Recently, Verde et al. (2002) computed the bispectrum of the 2dF Galaxy Redshift Survey, and concluded that the non-linear bias is consistent with zero. The other complementary approach to quantify the non-Gaussianity in the SDSS galaxies by means of topological analysis (i.e., in terms of the Minkowski functionals) was already conducted (Hoyle et al. 2002; Hikage et al. 2002, 2003). The above results are largely consistent with that predicted from purely gravitational nonlinearity, while a weak morphological difference is marginally detected (e.g., figure 13 of Hikage et al. 2003). Here, we report on the first results of characterizing the non-Gaussianity in the SDSS galaxy samples using 3PCFs in redshift space. In particular, we consider the dependence of 3PCFs on the morphology, color, and luminosity of galaxies by constructing volume-limited samples so as to avoid possible systematics due to the selection function. A separate companion paper by Nichol et al. (in preparation) focuses on a detailed comparison of 3PCFs between the 2dF (Jing, Börner 2004) and the SDSS galaxies.

The paper is organized as follows: section 2 describes our volume-limited sample of SDSS galaxies and the morphology and color classification methods. The measurements of 3PCFs are detailed in section 3 with particular attention given to their dependence on the morphology, color and luminosity of galaxies. Finally, we summarize the results in section 4. We compare several different estimators of 2PCFs and 3PCFs in Appendix. Throughout the data analysis, we adopt the following set of cosmological parameters: the matter density parameter, $\Omega_m = 0.3$; the dimensionless cosmological constant, $\Omega_\Lambda = 0.7$; and the Hubble constant in units of 100km/s/Mpc, $h = 0.7$.

2. Volume-Limited Samples of SDSS Galaxies

It is expected that galaxy clustering depends on the intrinsic properties of the galaxy samples under consideration, including their morphological types, colors, and

luminosities. Therefore, a straightforward analysis of magnitude-limited samples must be interpreted with caution because several different effects may be simultaneously involved. The magnitude-limited sample of SDSS galaxies enables us to construct volume-limited samples of different luminosities, morphologies and colors. This essentially removes the above difficulties while keeping a statistically significant number of galaxies in each sample.

Our present analysis is based on a subset of the SDSS galaxy redshift data, ‘Large-scale Structure Sample 12’ (Blanton et al. in preparation), which is larger by a factor of 1.8 than the public Data Release One (Abazajian et al. 2003). This sample includes galaxies with r -band magnitudes of between 14.5 and 17.77 after correction for Galactic reddening using the maps of Schlegel, Finkbeiner, and Davis (1998). For more details, the following can be consulted: York et al. (2000) for an overview of the SDSS; Gunn et al. (1998) for a description of the photometric camera; Stoughton et al. (2002) for photometric analysis; Fukugita et al. (1996), Hogg et al. (2001), and Smith et al. (2002) for the photometric system; Pier et al. (2003) for the astrometric calibration; Eisenstein et al. (2001); Strauss et al. (2002) for selection of the galaxy spectroscopic samples; and Blanton et al. (2003) for spectroscopic tiling.

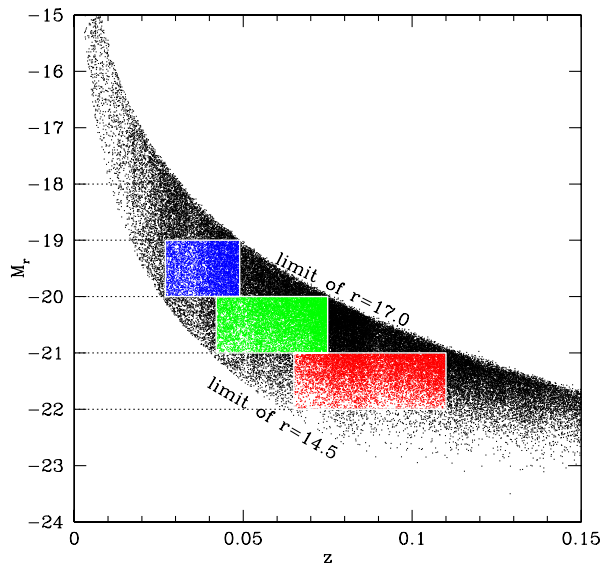


Fig. 1. Redshift - absolute magnitude relation for volume-limited samples of galaxies with $14.5 < r < 17.0$.

We construct two different kinds of volume-limited samples: one is based on the morphological classification, and the other is on the color of galaxies (figure 1 and table 1). Figure 2 illustrates the distribution of those galaxies in a volume-limited sample.

Following Shimasaku et al.(2001), we classify the morphology of galaxies according to the (inverse) concentration index (c_i), which denotes the ratio of the half-light Petrosian radius to the 90%-light Petrosian radius.

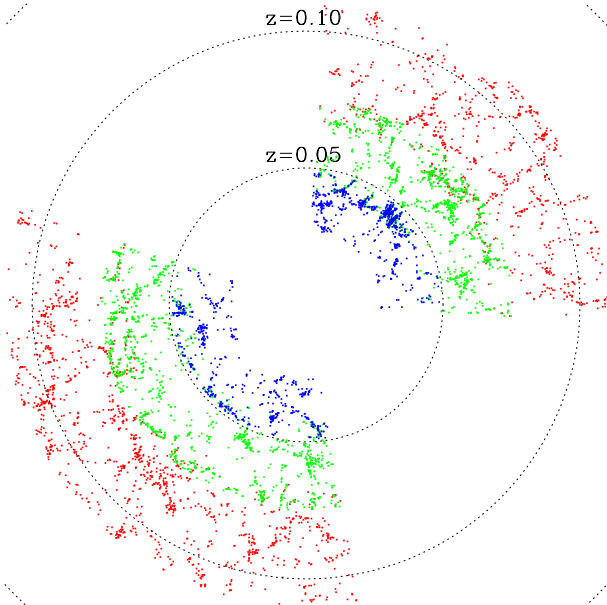


Fig. 2. Distribution of galaxies in the volume-limited samples ($14.5 < r < 17.0$; see table 1 and figure 1).

Table 1. Volume-limited samples of SDSS galaxies; $14.5 < r < 17.0$ for the early/late classification and $14.5 < r < 17.5$ for color classification.

$M_r - 5 \log h$	z	early	late
-22 to -21	0.065-0.11	5881	3897
-21 to -20	0.042-0.075	5115	5975
-20 to -19	0.027-0.049	1626	3965

$M_r - 5 \log h$	z	red	blue
-22 to -21	0.065-0.14	7949	8329
-21 to -20	0.042-0.093	8930	8155
-20 to -19	0.027-0.061	3706	3829

Specifically, we define galaxies with $c_i \leq c_{i,c}$ as early-types, and those with $c_i \geq c_{i,c}$ as late-types. The critical value $c_{i,c} = 0.35$ is adopted for galaxies with $r < 16.0$. Figure 3 shows the completeness and contamination of this classification scheme. Around $c_i \sim 0.35$ the completeness reaches 80% and the contamination goes below 20%. The classification based on c_i is affected by the fact that the image quality of SDSS galaxies with $r > 16.0$ starts to be degraded due to the seeing. In order to empirically compensate for the effect, we slightly change the critical value: $c_{i,c} = 0.359$ for $16.0 < r \leq 16.5$ and $c_{i,c} = 0.372$ for $16.5 < r \leq 17.0$. Those values are chosen so that the number ratio of early- to late-types remains the same in the three different magnitude ranges: $14.0 < r < 16.0$, $16.0 < r \leq 16.5$, and $16.5 < r \leq 17.0$. We do not classify the morphology of galaxies with $r > 17.0$.

On the other hand, classification of galaxies according to their colors does not require such a good image quality as the c_i classification. Thus, we can make use of galaxies down to $r = 17.5$, leading to an improved statistical

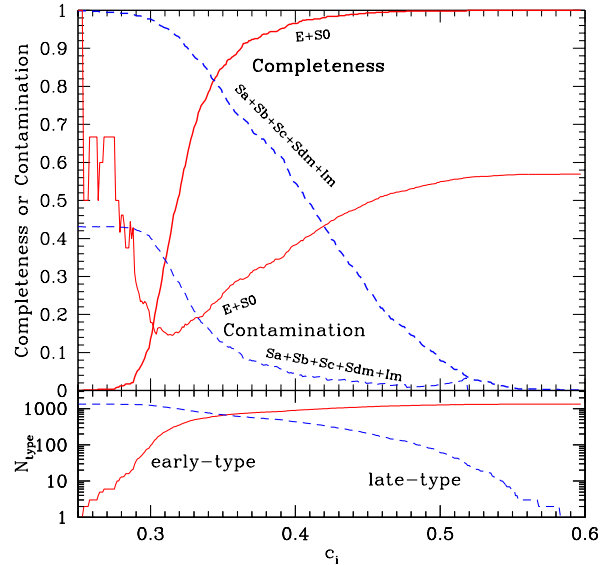


Fig. 3. Completeness of morphological classification according to the inverse concentration parameter.

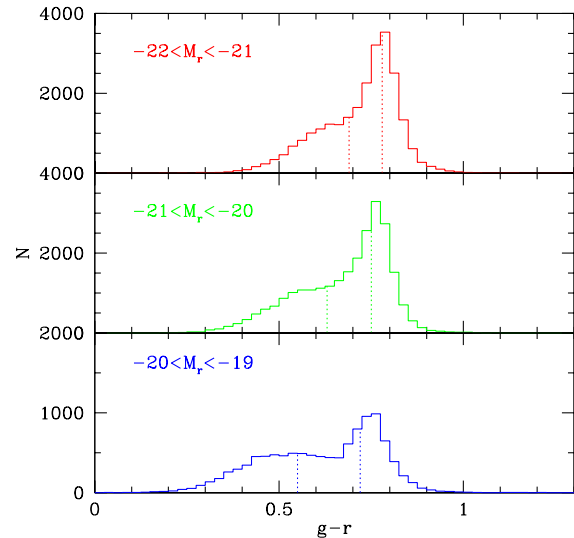


Fig. 4. Histograms of the color distribution for three volume-limited galaxy samples (table 1). The bin of histogram is $\Delta(g-r) = 0.025$. The dotted vertical lines in each panel indicate the color thresholds that divide galaxies in three different color subsamples.

significance. Figure 4 shows the distribution of $g-r$ for volume-limited galaxies corresponding to the lower part of table 1. Clearly, the colors are strongly correlated with the luminosity, and several different versions of color-selected samples are possible. Since our goal is to see if galaxy clustering is dependent on the colors in a complementary manner to the previous morphological classification, we divided each volume-limited sample into three subsamples that roughly have equal numbers of galaxies. More

precisely, we defined red (blue) galaxies as $g-r > 0.78$, > 0.75 , and > 0.72 ($g-r < 0.69$, < 0.63 , and < 0.55) for $-22 < M_r - 5 \log h < -21$, $-21 < M_r - 5 \log h < -20$, and $-20 < M_r - 5 \log h < -19$, respectively. Here, g and r are k -corrected magnitudes. These thresholds are indicated in the vertical lines in figure 4. Figure 5 illustrates the relations between our two classification schemes.

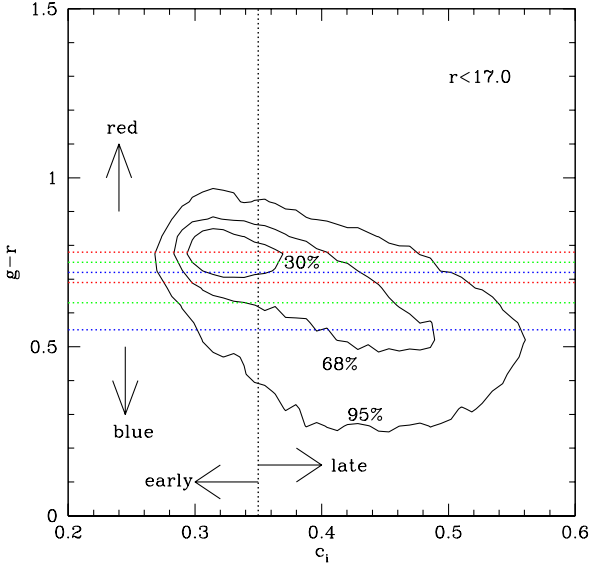


Fig. 5. Relation between the colors and the inverse concentration parameters of galaxies. The horizontal dotted lines correspond to the vertical dotted lines in figure 4.

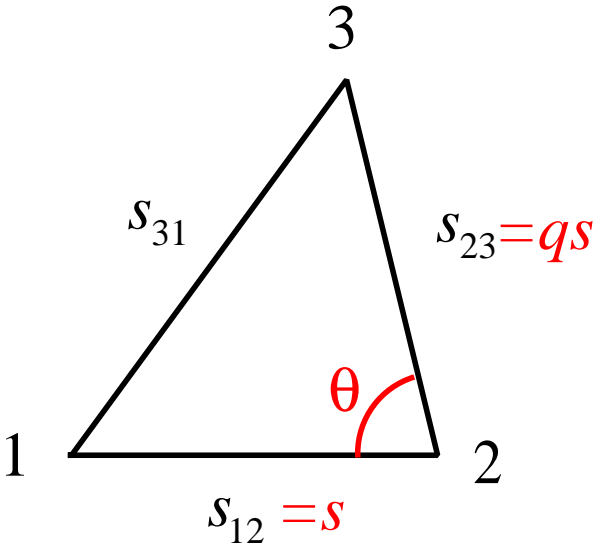


Fig. 6. Parameters to define the shape of triangles.

3. Measurements and Results

3.1. Counting Triplets

In the present analysis, we directly computed the number of triplets to estimate the 3PCFs $\zeta(s_{12}, s_{23}, s_{31})$ in redshift space. In this way, we properly take account of the complicated survey volume boundary. To be more specific, we distributed N_R random particles over the survey volume of a given sample of N_D galaxies, following the selection function of the latter (we used $N_R = 25N_{D,\text{all}}$, where $N_{D,\text{all}}$ is the number of all galaxies in each luminosity bin). Then, the 3PCFs were computed from the following estimator (Szapudi, Szalay 1998):

$$\begin{aligned} \zeta(s_{12}, s_{23}, s_{31}) &= \frac{DDD(s_{12}, s_{23}, s_{31})}{RRR(s_{12}, s_{23}, s_{31})} - 3 \frac{DDR(s_{12}, s_{23}, s_{31})}{RRR(s_{12}, s_{23}, s_{31})} \\ &+ 3 \frac{DRR(s_{12}, s_{23}, s_{31})}{RRR(s_{12}, s_{23}, s_{31})} - 1, \end{aligned} \quad (2)$$

where DDD , DDR , DRR , and RRR are the number of corresponding triplets consisting of galaxies and random particles, and are normalized by $N_D(N_D-1)(N_D-2)/6$, $N_D(N_D-1)N_R/2$, $N_D N_R(N_R-1)/2$, and $N_R(N_R-1)(N_R-2)/6$, respectively. The above estimator is close to optimal, because it is constructed to provide accurate edge effect corrections. We decided to use the Szapudi and Szalay estimator, since we found that it converges the true 3PCF slightly more rapidly than the estimator of Jing and Börner (1998) with the given number of random particles (see Appendix for details). We also estimated the redshift space 2PCF with the analogous estimator (Landy, Szalay 1993), and defined the normalized amplitude of 3PCFs as

$$Q_z(s_{12}, s_{23}, s_{31}) \equiv \frac{\zeta(s_{12}, s_{23}, s_{31})}{\xi(s_{12})\xi(s_{23}) + \xi(s_{23})\xi(s_{31}) + \xi(s_{31})\xi(s_{12})}. \quad (3)$$

Two different parameterizations of triangular shape are conventionally used in this field. One is

$$s_{12} = s, \quad s_{23} = us, \quad s_{31} = (u+v)s, \quad (4)$$

where $s_{12} \leq s_{23} \leq s_{31}$ is assumed (thus $u \geq 1$ and $0 \leq v < 1$). The other is

$$s_{12} = s, \quad s_{23} = qs, \quad s_{31} = s\sqrt{1+q^2-2q\cos\theta}, \quad (5)$$

where $s_{12} \leq s_{23}$ is assumed (thus, $q \geq 1$, but s_{31} may be smaller than either of the other two; see figure 6). Note that according to the second parameterization, one triangle is counted in three different bins in (s, q, θ) . Although the first parameterization is more traditional in the real data analysis, we adopt the second, which is widely used in theoretical predictions. More specifically, we choose 8 equally-spaced logarithmic bins in $0.4h^{-1}\text{Mpc} \leq s < 10.0h^{-1}\text{Mpc}$ and 5 equally-spaced linear bins both in $1 \leq q < 5$ and in $0 < \theta < \pi$. Since the number of triplets of $s < 1.0h^{-1}\text{Mpc}$ is very small (typically $DDD \lesssim 50$), we plot the 3PCFs only for $s > 1.0h^{-1}\text{Mpc}$ (where we have more than 100 DDD counts) in what follows. Also, the errors quoted below are evaluated from the 16 jack-knife re-sampling (see e.g., Lupton 1993).

3.2. Equilateral Triangles

We ignore any possible dependence on the triangular shape for the moment, and first consider 3PCFs for equilateral triangles in detail. For this purpose, we first directly evaluate the lengths of three sides of triplets. If those sides fall in the same bin among 8 equally-spaced logarithmic bins between $0.4h^{-1}\text{Mpc}$ and $10.0h^{-1}\text{Mpc}$, we define the triplets as being equilateral triangles. Figures 7, 8, and 9 show Q_z over $1h^{-1}\text{Mpc} < s < 10h^{-1}\text{Mpc}$. The overall conclusion is that Q_z is almost scale-independent and ranges between 0.5 and 1.0, and no systematic dependence is noticeable on the luminosity, morphology, and color.

Previous simulations and theoretical models (Suto 1993; Matsubara, Suto 1994, Matsubara 1994, Takada, Jain 2003) indicate that Q decreases with the scale in both real and redshift spaces. Observationally, Jing and Börner (2003) suggested that Q_z of the 2dF galaxies also decreases as scale. Neither trend is clear in the results. This might be partly due to the different velocity dispersion of the galaxies in the two samples. Jing, Mo, and Börner (1998) reported that the early spirals (Sa, Sab, Sb) have a significantly smaller Q than the other types, which is qualitatively consistent with the present results.

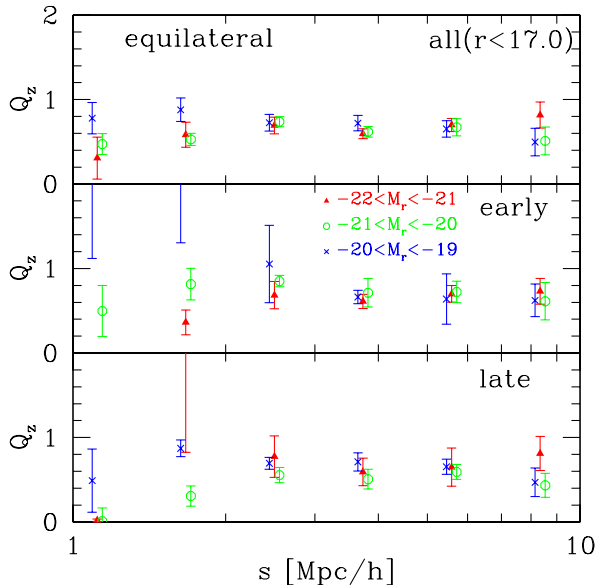


Fig. 7. Luminosity dependence of the normalized amplitude of three-point correlation functions classified according to the morphologies of galaxies. Only equilateral triangles are considered. Different symbols correspond to different luminosities: $-22 < M_r - 5 \log h < -21$ by solid triangles, $-21 < M_r - 5 \log h < -20$ by open circles, and $-20 < M_r - 5 \log h < -19$ by crosses. Top: all galaxies, Middle: early-type galaxies, Bottom: late-type galaxies.

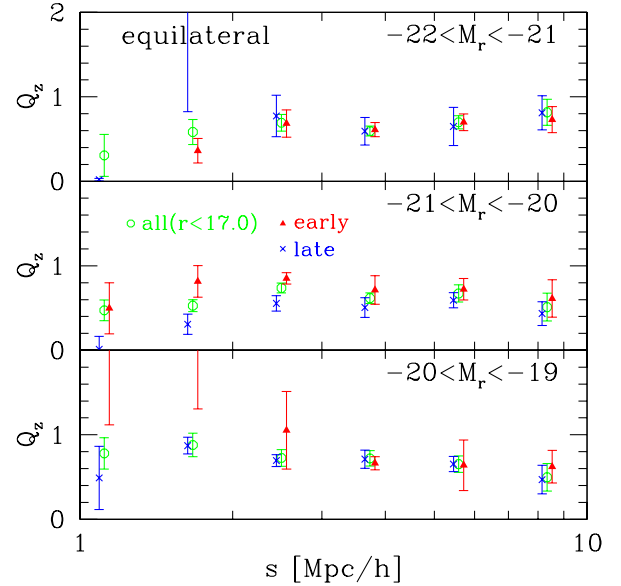


Fig. 8. Same as figure 7, but different symbols corresponds to different morphologies; all galaxies in open circles, early-type galaxies in solid triangles, and late-type galaxies in crosses. Top: $-22 < M_r - 5 \log h < -21$, Middle: $-21 < M_r - 5 \log h < -20$, Bottom: $-20 < M_r - 5 \log h < -19$.

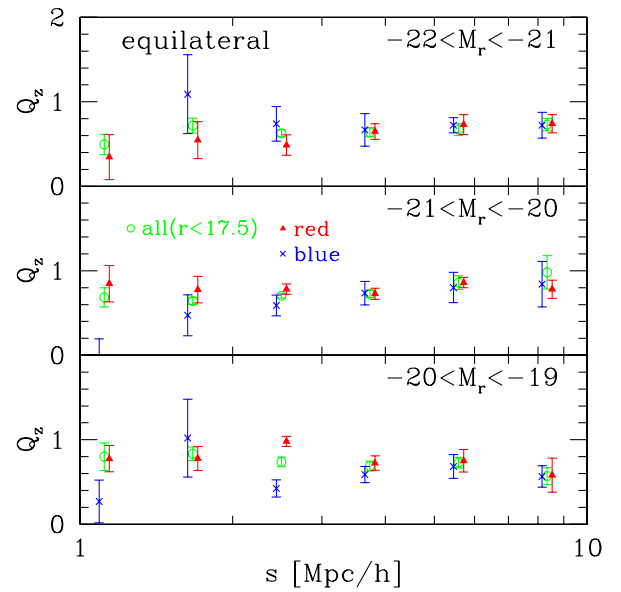


Fig. 9. Same as figure 8, but for classification according to the colors of galaxies. All galaxies by open circles, red galaxies by solid triangles, and blue galaxies by crosses.

3.3. Relation to Biasing of the Two-Point Correlation Function

The statement that the values of Q_z are insensitive to the intrinsic properties of galaxies may sound somewhat misleading. The reduced three-point correlation amplitude is normalized by the square of the 2PCFs for the corresponding galaxies. This implies that the (unreduced)

3PCF depends on the galaxy properties, since 2PCFs are known to show a clear dependence on the luminosity, color, and morphology of galaxies (e.g., Lahav and Suto 2003 for a recent review). In order to further demonstrate the expected dependence in the current samples, we compute the biasing parameters estimated from the 2PCFs,

$$b_{z,i}(s) \equiv \sqrt{\frac{\xi_{z,i}(s)}{\xi_{z,\Lambda\text{CDM}}(s)}}, \quad (6)$$

where the index i runs over each sample of galaxies with different morphologies, colors, and luminosities. The predictions of the mass 2PCFs in redshift space, $\xi_{z,\Lambda\text{CDM}}(s)$, in the Λ Cold Dark Matter model are computed by properly taking account of the light-cone effect over the corresponding redshift range (Hamana et al. 2001). In doing so, we adopt the fluctuation amplitude $\sigma_8 = 0.9$ and the one-dimensional peculiar pairwise velocity dispersion of 800km/s in addition to our fiducial set of cosmological parameters.

As an illustrative example, consider a simple bias model in which the galaxy density field, $\delta_{g,i}$, for the i -th population of galaxies is given by

$$\delta_{g,i} = b_{g,i(1)}\delta_{\text{mass}} + b_{g,i(2)}\delta_{\text{mass}}^2. \quad (7)$$

If both $b_{g,i(1)}$ and $b_{g,i(2)}$ are constant and the mass density field $\delta_{\text{mass}} \ll 1$, equation (3) implies that

$$Q_{g,i} = \frac{1}{b_{g,i(1)}}Q_{\text{mass}} + \frac{b_{g,i(2)}}{b_{g,i(1)}^2}. \quad (8)$$

Thus, the linear bias model ($b_{g,i(2)} = 0$) simply implies that $Q_{g,i}$ is inversely proportional to $b_{g,i(1)}$. While this simple model may not be accurately applicable on the scales of our results, it is instructive to plot $1/b_{g,i}$ deduced from the 2PCF of galaxies with different luminosities and morphologies. The results are shown in figures 10, 11, and 12. A linear bias model would predict that the ratio of Q_z of early-types and late-types is $Q_{z,\text{early}}/Q_{z,\text{late}} = b_{\text{late}}/b_{\text{early}} \approx 0.8$, and similarly that $Q_{z,\text{red}}/Q_{z,\text{blue}} = b_{\text{blue}}/b_{\text{red}} \approx 0.5$. Neither figure 8 nor 9, however, shows such systematic trends within our ~ 20 percent measurement accuracy. In a sense, the biasing in the 3PCFs seems to compensate for the difference of Q_g purely due to that in the 2PCFs. Such a behavior is unlikely to be explained by any simple model inspired by the perturbative expansion, like equation (7). Rather, it indeed points to a kind of regularity or universality of the clustering hierarchy behind galaxy formation and evolution processes. At least we can conclude that the galaxy biasing is more complex than the simple deterministic and linear model. More precise measurements of 3PCFs, and even higher order statistics with future SDSS datasets would indeed be valuable to gain more specific insights into the empirical biasing model.

3.4. Shape Dependence

Next consider the dependence of the 3PCFs on the triangular shape. For this purpose, we consider the

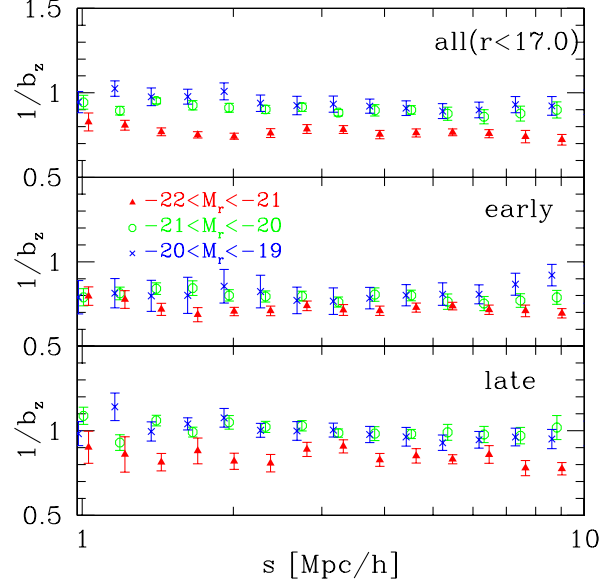


Fig. 10. Inverse of the biasing parameters of the two-point correlation functions plotted in the same way as in figure 7.

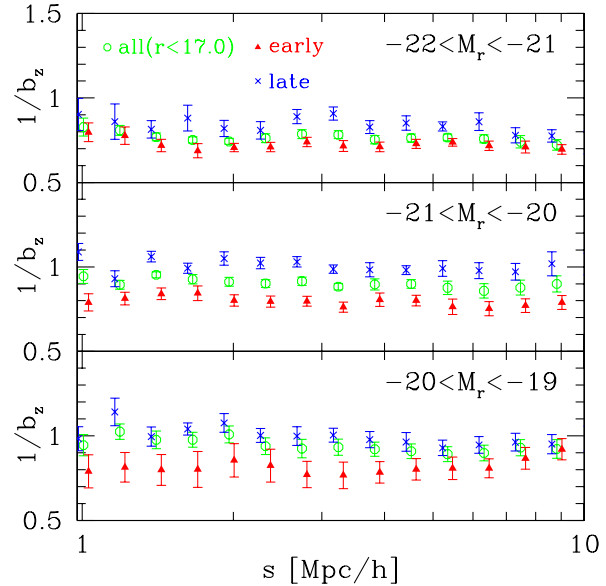


Fig. 11. Inverse of biasing parameters of the two-point correlation functions plotted in the same way as in figure 8.

volume-limited samples classified according to the colors ($r < 17.5$) because they have a greater number of galaxies. Figure 13 shows Q_z for all, red, and blue galaxies with $-21 < M_r - 5 \log h < -20$ separately. Those plots indicate a weak θ -dependence expected from the previous perturbation theory and N-body simulations (e.g., Barriga, Gaztañaga 2002; Takada, Jain 2003). The θ -dependence is weaker on nonlinear scales ($s < 1h^{-1}\text{Mpc}$), and becomes noticeable on larger scales. While the amplitudes of Q_z are much smaller than, and the color dependence seems very different from the corresponding prediction (figure

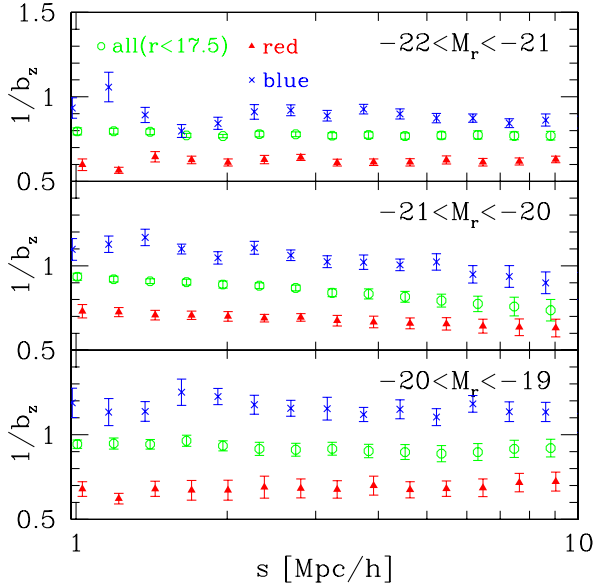


Fig. 12. Inverse of biasing parameters of the two-point correlation functions plotted in the same way as in figure 9.

17 of Takada, Jain 2003), they adopt a simple halo approach, and our color selection criteria are not necessarily the same as theirs; further careful study is needed to understand the origin of the difference (after the present paper is accepted, Wang et al. 2004 submitted a theoretical paper applying the halo model to account for the 3PCFs of 2dF galaxies, in particular their dependence on types and luminosity dependences, and shows the possibility that the halo model can match the observation).

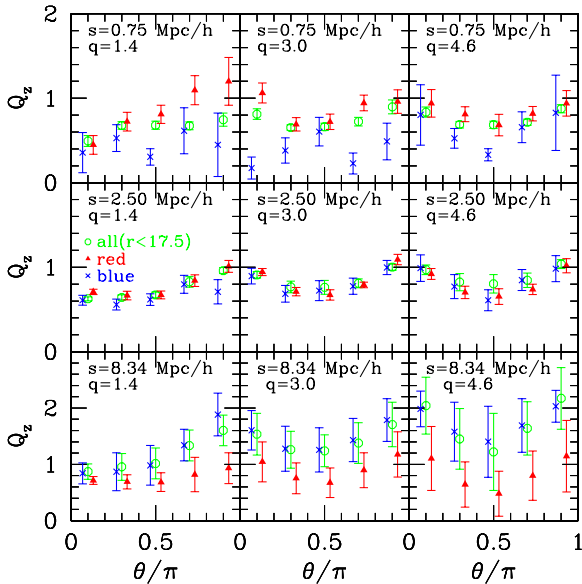


Fig. 13. Shape dependence of Q_z of volume-limited samples of galaxies with $r < 17.5$ and $-21 < M_r - 5 \log h < -20$ (classified according to their color).

4. Summary and Discussion

We have presented the first detailed study of the three-point correlation function of SDSS galaxies in redshift space. We examined the dependence of their reduced amplitudes, Q_z , [eq.(3)] on the scale and shape of the triangles for various volume-limited samples with different morphologies, colors, and luminosities. As for equilateral triangles, we basically confirm the hierarchical clustering relation for scales of $1h^{-1}\text{Mpc} < s < 10h^{-1}\text{Mpc}$. On the other hand, Q_z shows significant shape dependence, as expected from perturbation theory and N-body simulations, particularly at large scale, although the amplitude of Q_z is much smaller than the expectation.

The most important finding is that although the two-point correlation functions of those galaxies show a clear dependence on their luminosity, morphology, and color, we did not find any robust dependence of Q_z on those properties; the Q_z results when taken alone imply that galaxies are faithful tracers of the underlying mass distribution, and that their intrinsic properties are independent of the purely nonlinear gravitational evolution. At the same time, however, their two-point correlation functions strongly indicate that they are biased tracers. If we attempt to reconcile these two behaviors by using a simple linear bias model, we cannot adjust it to simultaneously explain both the two-point correlation functions and the insensitivity of Q_z on the galaxy properties. This implies that the galaxy biasing is non-linear and fairly complex, while nonetheless displaying a remarkable constancy in reduced amplitudes.

The above conclusion may appear to be inconsistent with the argument of Verde et al. (2002), who concluded that the non-linearity in 2dF galaxy biasing is negligible from the bispectrum analysis. We note, however, that they did not attempt to divide those galaxies into different subsamples. If we look at the results of all galaxies alone, top-panels of figures 7 and 10 may indicate the same conclusion as reached by Verde et al. (2002). In other words, our empirical finding indicates that the non-linearity of the biasing, b_2 , of galaxies vanishes when the corresponding linear biasing parameter, b_1 , is unity. The fact that the two parameters, b_1 and b_2 , are highly correlated with each other is qualitatively consistent with some biasing model predictions including halo models or peak models (Mo et al. 1997). It is remarkable that the current galaxy survey approaches the level of discussing the validity of those models quantitatively. Future SDSS datasets with more area and a larger number of galaxies will be able to place stronger limits on this observation. This in turn will be useful for a detailed understanding of the nature of galaxy biasing.

We thank Y.P. Jing and Gerhard Börner for useful correspondences on their measurements of three-point correlation functions of 2dF galaxies and an anonymous referee for his/her useful comments. I. K. gratefully acknowledges support from the Takenaka-Ikueikai fellowship. He enjoyed the hospitality at Carnegie Mellon

University and University of Pittsburgh where part of this work was done, and thanks the Hayakawa fund of Astronomical Society of Japan for the travel support. Numerical computations were carried out at ADAC (Astronomical Data Analysis Center) of the National Astronomical Observatory of Japan, and also at computer facilities at the University of Tokyo supported by the Special Coordination Fund for Promoting Science and Technology, Ministry of Education, Culture, Sports, Science and Technology. IS and JP was supported by NASA through AISR NAG5-11996, and ATP NASA NAG5-12101 as well as by NSF grants AST02-06243 and ITR 1120201-128440.

Funding for the creation and distribution of the SDSS Archive has been provided by the Alfred P. Sloan Foundation, the Participating Institutions, the National Aeronautics and Space Administration, the National Science Foundation, the U.S. Department of Energy, the Japanese Monbukagakusho, and the Max Planck Society. The SDSS Web site is <http://www.sdss.org/>.

The SDSS is managed by the Astrophysical Research Consortium (ARC) for the Participating Institutions. The Participating Institutions are The University of Chicago, Fermilab, the Institute for Advanced Study, the Japan Participation Group, The Johns Hopkins University, Los Alamos National Laboratory, the Max-Planck-Institute for Astronomy (MPIA), the Max-Planck-Institute for Astrophysics (MPA), New Mexico State University, University of Pittsburgh, Princeton University, the United States Naval Observatory, and the University of Washington.

Appendix. Comparison of the Estimators of Two- and Three-Point Correlation Functions

For an accurate determination of the normalized amplitudes of Q , we need reliable estimators for the two- and three-point correlation functions. For this purpose, we use a set of data particles ($N_D = 64^3$; generated from a N-body simulation with 256^3 dark matter particles; Jing and Suto 1998) distributed in a cube of $V_{\text{box}} = (100h^{-1}\text{Mpc})^3$. We then compare the following three estimators for 2PCFs:

$$\xi_{\text{direct}} = \frac{DD}{V_{12}/V_{\text{box}}} - 1, \quad (\text{direct}); \quad (\text{A1})$$

$$\xi_{\text{H}} = \frac{DD \cdot RR}{[DR]^2} - 1, \quad (\text{Hamilton 1993}); \quad (\text{A2})$$

$$\xi_{\text{LS}} = \frac{DD - 2DR + RR}{RR}, \quad (\text{Landy, Szalay 1993}); \quad (\text{A3})$$

where V_{12} denotes the volume of the spherical shell with the thickness of the corresponding separation bin, and DD , DR , and RR are the number of corresponding pairs of data and random particles, and are normalized by $N_D(N_D - 1)/2$, $N_D N_R$, and $N_R(N_R - 1)/2$, respectively.

Similarly, we use the following estimators for the 3PCFs:

$$\zeta_{\text{direct}} = \frac{DDD}{V_{123}^2/V_{\text{box}}^2} - 3\xi_{\text{direct}} - 1, \quad (\text{A4})$$

$$\zeta_{\text{JB}} = \frac{[RRR]^2 DDD}{[DRR]^3} - \frac{3RRR \cdot DDR}{[DRR]^2} + 2, \quad (\text{A5})$$

$$\zeta_{\text{SS}} = \frac{DDD - 3DDR + 3DRR - RRR}{RRR}. \quad (\text{A6})$$

The first uses the analytical expression for the effective volume squared for the equilateral triplets. If one considers the size of the the equilateral triplets between r_{min} and r_{max} , it is simply given by

$$V_{123}^2 = \pi^2 (r_{\text{max}}^2 - r_{\text{min}}^2)^3. \quad (\text{A7})$$

Because similar expressions in an arbitrary survey volume shape are not available analytically, we focus on the equilateral triplets in periodic cube of simulations. The latter two correspond to estimators by Jing and Börner (1998) and Szapudi and Szalay (1998), respectively. The combination of terms in Jing and Börner (1998) comes from the fact that the first term corresponds to $1 + \xi(r_{12}) + \xi(r_{23}) + \xi(r_{31}) + \zeta(r_{12}, r_{23}, r_{31})$, and the second term to $3 + \xi(r_{12}) + \xi(r_{23}) + \xi(r_{31})$, yielding the desired ζ mathematically.

The results of the convergence test are shown in Figure 14 for 2PCFs and Figure 15 for 3PCFs. These figures show the ratios of the two different estimators with various N_R against the “direct” estimates [equations (A1) and (A4)] which do not use the random particles. With this number of random particles, equations (A3) and (A6) reproduce the “direct” results within $\sim 5\%$ for 2PCFs and 3PCFs, respectively.

Figure 14 indicates that ξ_{LS} converges to the true value (ξ_{direct}) more rapidly even with a smaller N_R than ξ_{H} (see also Kerscher et al. 2000). Figure 15 shows that the estimators of 3PCFs are generally less stable compared with those of 2PCFs. Still, ζ_{SS} seems better behaved than ζ_{JB} . Thus, we adopted ξ_{LS} and ζ_{SS} in the present analysis.

References

- Abazajian, K., et al. 2003, AJ, 126, 2081 (Data Release One)
- Barriga, J., & Gaztañaga, E. 2002, MNRAS, 333, 443
- Bean, A. J., Efstathiou, G., Ellis, R. S., Peterson, B. A., & Shanks, T. 1983, MNRAS, 205, 605
- Blanton, M. R., Lin, H., Lupton, R. H., Maley, F. M., Young, N., Zehavi, I., & Loveday, J. 2003, AJ, 125, 2276
- Eisenstein, D. J., et al. 2001, AJ, 122, 2267
- Fry, J. N. 1984, ApJ, 279, 499
- Fukugita, M., Ichikawa, T., Gunn, J. E., Doi, M., Shimasaku, K., & Schneider, D. P. 1996, AJ, 111, 1748
- Groth, E.J., & Peebles, P.J.E. 1977, ApJ, 217, 385
- Gunn, J. E., et al. 1998, AJ, 116, 3040
- Hale-Sutton, D., Frong, R., Metcalfe, N., & Shanks, T. 1989, MNRAS, 237, 569
- Hamana, T., Colombi, S., & Suto, Y. 2001, A&A, 367, 18
- Hamilton, A.J.S. 1993, ApJ, 417, 19
- Hikage, C., et al. 2002, PASJ, 54, 707
- Hikage, C., et al. 2003, PASJ, 55, 911
- Hogg, D. W., Finkbeiner, D. P., Schlegel, D. J., & Gunn, J. E. 2001, AJ, 122, 2129
- Hoyle, F., et al. 2002, ApJ, 580, 663

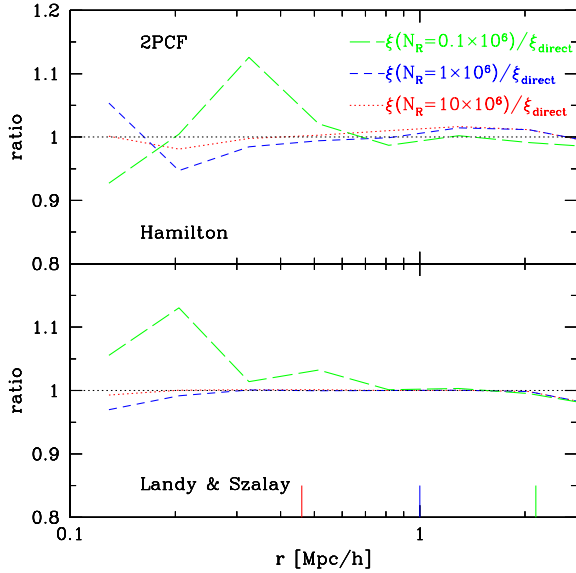


Fig. 14. Comparison of the three estimators of 2PCFs with a different number of random particles (N_R). The small bars in the bottom panel indicate the mean separation length of random particles for different N_R . Upper: the dependence of the Hamilton estimator on the number of random particles. The long-dashed, short-dashed, and dotted curves denote $\xi_H(N_R = 0.1 \times 10^6)/\xi_{\text{direct}}$, $\xi_H(N_R = 1 \times 10^6)/\xi_{\text{direct}}$ and $\xi_H(N_R = 10 \times 10^6)/\xi_{\text{direct}}$, respectively. Lower: same as the upper panel, but for the Landy–Szalay estimator.

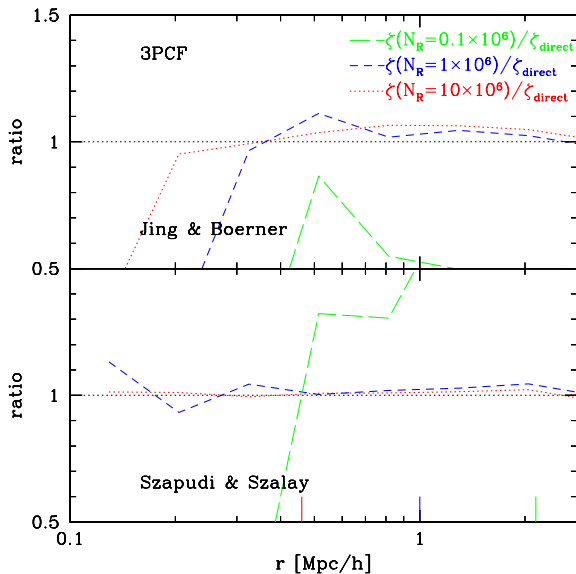


Fig. 15. Same as figure 14, but for 3PCFs.

Jing, Y. P., & Börner, G. 1998, *ApJ*, 503, 37
 Jing, Y.P., & Börner, G. 2003, *ApJ*, submitted (astro-ph/0311585)
 Jing, Y.P., Mo, H.J., & Börner, G. 1991, *A&A*, 252, 449
 Jing, Y.P., & Suto, Y. 1998, *ApJ*, 494, L5
 Kerscher, M., Szapudi, I., & Szalay, A.S. 2000, *ApJ*, 535, L13
 Komatsu, E., et al. 2003, *ApJS*, 148, 119

Lahav, O., & Suto, Y. 2003, *Living Rev. Relativity*, in press (Max-Planck-Gesellschaft, astro-ph/0310642)
 Landy, S.D., & Szalay, A.S. 1993, *ApJ*, 412, 64
 Lupton, R. 1993, *Statistics in Theory and Practice* (Princeton: Princeton Univ. Press)
 Matsubara, T. 1994, *ApJ*, 424, 30
 Matsubara, T., & Suto, Y. 1994, *ApJ*, 420, 497
 Mo, H.J., Jing, Y.P., & White, S.D.M. 1997, *MNRAS*, 284, 189
 Peebles, P.J.E., & Groth, E.J. 1975, *ApJ*, 196, 1
 Pier, J. R., Munn, J. A., Hindsley, R. B., Hennessy, G. S., Kent, S. M., Lupton, R. H., & Ivezić, Ž., 2003, *AJ*, 125, 1559
 Schlegel, D. J., Finkbeiner, D. P., & Davis, M. 1998, *ApJ*, 500, 525
 Shimasaku, K., et al. 2001, *AJ*, 122, 1238
 Smith, J. A., et al. 2002, *AJ*, 123, 2121
 Stoughton, C., et al. 2002, *AJ*, 123, 485
 Strauss, M. A., et al. 2002, *AJ*, 124, 1810
 Suto, Y. 1993, *Prog.Theor.Phys.*, 90, 1173
 Suto, Y., & Matsubara, T. 1994, *ApJ*, 420, 504
 Szapudi, I., & Szalay, A. S. 1998, *ApJ*, 494, L41
 Szapudi, I., et al. 2002, *ApJ*, 570, 75
 Takada, M., & Jain, B. 2003, *MNRAS*, 340, 580
 Verde, L., et al. 2002, *MNRAS*, 335, 432
 Wang, Y., Yang, X., Mo, H. J., van den Bosch, F. C., & Chu, Y. Q. 2004, astro-ph/0404143
 York, D. G., et al. 2000, *AJ*, 120, 1579.